

Modeling and detection of quasi-static nanotesla magnetic field variations using magnetoelectric laminate sensors

This article has been downloaded from IOPscience. Please scroll down to see the full text article.

2008 Meas. Sci. Technol. 19 015206

(<http://iopscience.iop.org/0957-0233/19/1/015206>)

View [the table of contents for this issue](#), or go to the [journal homepage](#) for more

Download details:

IP Address: 128.104.1.219

The article was downloaded on 08/07/2012 at 13:24

Please note that [terms and conditions apply](#).

Modeling and detection of quasi-static nanotesla magnetic field variations using magnetoelectric laminate sensors

Z P Xing¹, J Y Zhai¹, S X Dong¹, J F Li¹, D Viehland¹
and W G Odendaal²

¹ Materials Science and Engineering, Virginia Tech, Blacksburg, VA 24061, USA

² Electrical Engineering, Virginia Tech, Blacksburg, VA 24061, USA

E-mail: xing@vt.edu

Received 20 June 2007, in final form 2 November 2007

Published 17 December 2007

Online at stacks.iop.org/MST/19/015206

Abstract

Laminated composites of magnetostrictive and piezoelectric layers have been developed for their magnetoelectric (ME) product tensor properties. In spite of the considerable progress in materials aspects, little attention has been given to ME laminate incorporation into a detection technology. Here, we present a ME technology including the laminate equivalent model, detection circuitry consideration and noise mitigation for ME laminate sensors operated at quasi-static (≤ 10 Hz) frequencies. We then constructed a passive magnetic field prototype sensor unit and detected a 2.6 nanotesla magnetic signal at 1 Hz frequency.

Keywords: magnetoelectric laminate sensor, quasi-static, modeling, nanotesla, low noise system

(Some figures in this article are in colour only in the electronic version)

1. Introduction

The magnetoelectric (ME) effect is defined as the polarization induced by a magnetic field (H) or the magnetization induced by an electric field (E) [1]. Composites consisting of magnetostrictive layers laminated together with piezoelectric ones have large ME effects, and have recently been the focus of investigations [2–9]. When an ac magnetic field (H_{ac}) is applied to these laminates, the magnetostrictive layer(s) elastically forces the piezoelectric layer(s) to strain, generating a piezoelectric charge.

To date, a number of investigations on the material aspects of the product tensor properties of ME laminates have been reported [4, 6, 10]. Applications in magnetic moment sensing via induced charge/voltage changes have been discussed [11, 12]; however, little attention has been given to the important considerations of the incorporation of the ME laminate in the circuit. Here, we present investigations of the ME laminate equivalent model, detection methodologies and circuit noise—emphasis is given to the sensing of quasi-static magnetic anomalies by a small battery operated device.

2. Equivalent model at low frequency and low H_{ac} ac magnetic field

We constructed a piece of Terfenol-D/Pb(Zr,Ti)O₃ (PZT)/Terfenol-D laminate operated in a longitudinal magnetization–transverse polarization (L–T) mode, as illustrated in figure 1. The laminate plane is in the (1, 2) plane. The PZT plane is polarized along the transverse direction (axis 3), while the Terfenol-D pieces are magnetized along the longitudinal direction (axis 2).

The piezoelectric PZT layer was an APC PZT-850 of dimensions $30 \times 6 \times 0.5$ mm³. The volume resistivity of the PZT layer was $\rho > 2 \times 10^{12}$ Ω m and its capacitance was ~ 3.8 nF; the sizes of the magnetostrictive Terfenol-D layers are $30 \times 6 \times 1$ mm³; and these layers were elastically bonded together using a high-strength epoxy.

The magnetostriction λ of Terfenol-D depends on H^2 , given as

$$\lambda = 1.5\lambda_s\mu_r^2M_s^{-2}H^2 = kH^2 \quad (1.1)$$

where λ_s and M_s are the saturation magnetostriction and magnetization, respectively; and μ_r is the weak-field relative

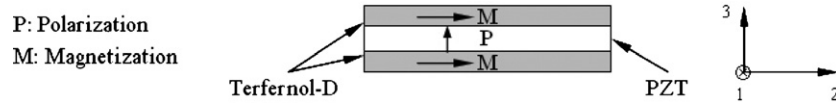


Figure 1. Structure of Terfermol-D/PZT/Terfermol-D.

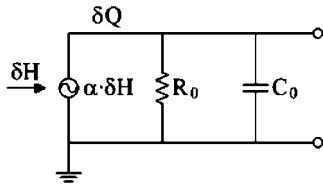


Figure 2. Equivalent ME laminate model at low frequency low applied ac magnetic field.

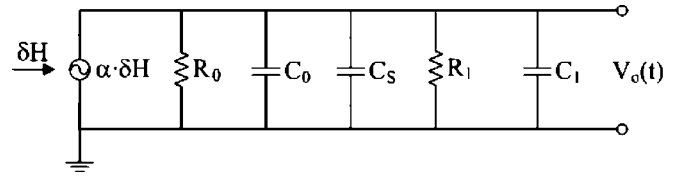


Figure 3. Equivalent detection circuit.

permeability of the magnetic phase, which is constant under small H_{ac} [13]. When an applied H_{ac} is much smaller than a simultaneously applied dc magnetic bias (H_{dc}), an effective piezomagnetic deformation is induced by H_{ac} , which can be obtained by the differentiation of (1.1) with respect to H , given as

$$\frac{\delta\lambda}{\delta H} \cong 2kH_{dc}. \quad (1.2)$$

In our laminate of figure 1, small magnetostrictive deformations ($\delta\lambda$) will elastically strain the piezoelectric layer (i.e., linear boundary condition). This results in a linear polarization change δP in the piezo layer and an induced charge $\delta Q = \delta PS$ (where S is the piezo-plate's surface area) across the piezo layer. Accordingly, the H -induced charge (δQ) is given as

$$\delta Q = \alpha \cdot \delta H = \alpha \cdot \delta H \quad (2)$$

where α is a constant at low H_{ac} and low drive frequency. From this equation, we can see that there should be linearity between the induced charge δQ and a small H_{ac} . A maximum piezomagnetic coefficient will occur when μ_r is a maximum in the $M-H$ curve (i.e., where the slope is highest): correspondingly, a maximum in the H -induced charge across the piezoelectric layer will also occur.

The piezoelectric layer of the ME laminates is capacitive, meaning we can consider the laminate as a capacitive source sensor. At low frequencies, a capacitive source sensor can be represented by a parallel equivalent circuit model, where a capacitor is in parallel with a large resistor [14]. Combining this approach with (2) above, we can simplify the equivalent circuit models for ME laminates for the case of low frequency ac magnetic fields, as given in figure 2, where C_0 and R_0 are the capacitance and resistance of the laminate, respectively, which are the same as those of the piezo layer. Since α is independent of the frequency in the sub-resonant range, this equivalent circuit can be used to linearly model the charge induced across the piezoelectric layer by low-frequency small ac magnetic fields in a time-domain mode, i.e., $Q(t) = \alpha H(t)$.

3. Low frequency detection considerations

Often, the ME effect in laminates has been reported as an H -induced voltage output from the piezo layer(s) [2–10]. This is consistent with (2), as the induced charge is proportional to the output voltage when the piezo layer(s) is open circuited, i.e., $V = Q/C$. However, in reality, some limitations must be imposed, as (i) any detection circuit will introduce some impedance, and thus the output voltage will not truly be measured in open-circuit conditions; and (ii) R_0 of the piezo layer is large and finite, but not infinite, and thus some leakage current will flow across the piezo layer at low frequencies, introducing error or drift into the measured value of the ME charge or voltage.

In the direct measurement method where the output of the ME sensor is directly connected to the oscilloscope (or some other similar instruments), the equivalent circuit can be depicted as given in figure 3, where C_s is any stray capacitance introduced by detection cables, R_1 and C_1 , respectively, are any input resistance and capacitance introduced by the oscilloscope.

The Laplace transform of the H -induced current $I(t)$ can then be expressed by

$$\begin{aligned} I(s) &= L(I(t)) = L\left(\frac{dQ(t)}{dt}\right) = sQ(s) - Q_0(s) \\ &= s\alpha H(s) - H_0(s) \end{aligned} \quad (3.1)$$

where $s = \sigma + j\omega$ is a complex frequency in complex nepers per second; here σ is the neper frequency in nepers per second and ω is the angular frequency in radians per second; $L(\sim)$ is the Laplace transform operation; and $Q(s)$ and $H(s)$ are the Laplace transforms of $Q(t)$ and $H(t)$, respectively. We can then choose the initial boundary condition in the s domain to make $H_0(s) = 0$ in equation (3.1). Thus, the transfer function $H_1(s)$ between the output voltage $V_o(s)$ and the input ac magnetic field $H(s)$ is

$$H_1(s) = \frac{V_o(s)}{H(s)} = \frac{s\alpha R'}{1 + sR'C'}, \quad (3.2)$$

where $R' = R_0R_1/(R_0 + R_1)$ and $C' = C_0 + C_1 + C_s$. Following (3.2), a Bode plot for $|H_1(j\omega)|$ is given in figure 4, where we can see that there is a zero point at $s = 0$ and a pole at $s = 1/R'C'$.

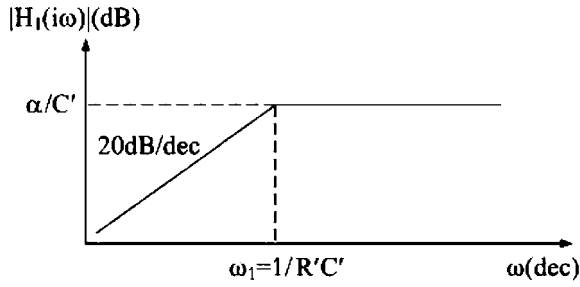
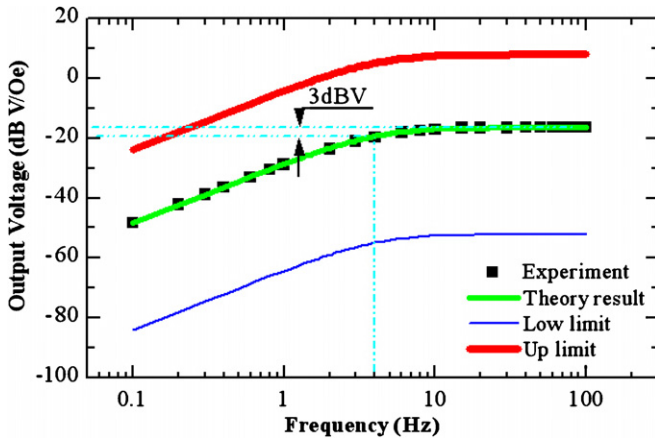

 Figure 4. Bode plot for $H_1(s)$.


Figure 5. ME direct measurement and theoretical predicted result.

A high cut-off frequency, f_h , above which the ME response is flat, can be calculated as $f_h = 1/(2\pi R'C')$. For the sample in figure 1, this high cut-off frequency is theoretically predicted to be about 4 Hz. However, in prior studies, this cut-off frequency is not reached until the Maxwell–Wagner relaxation region [15], which is in the μHz range for PZT850. To test our prediction, a direct measurement was carried out by placing the ME sensor at the center of a Helmholtz coil and by applying a small ac magnetic field (H_{ac}) along the longitudinal direction of the sensor. A dc magnetic bias (H_{dc}) was superimposed on H_{ac} along that same direction. The voltages induced across the PZT layer(s) were then measured by an oscilloscope. The experimental results and a theoretical prediction are given in figure 5. We can see that the experimental results match the predicted one quite well. The upper and lower limit curves in this figure that represent what we might consider good (10 nC Oe^{-1}) and bad (10 pC Oe^{-1}) values for ME coefficients are also illustrated. Our finding shows that the ME model of figure 2 is quite suitable for real detection circuitry considerations.

Another method for ME sensor detection is the use of a differential (or instrumentation) amplifier. The choice of the differential amplifier is restricted by the bias current I_b . The dc resistance R of the ME sensor in figure 1 is greater than $3 \times 10^{12} \Omega$, and the bias current I_b should satisfy the following requirement:

$$I_b \ll G \frac{V_s}{R}, \quad (4.1)$$

where V_s is the saturation output voltage of the instrumentation amplifier and G is the gain of the amplifier. Generally, V_s is about several volts (we choose $V_s = 3 \text{ V}$ for convenience) and G is generally greater than 10. So I_b should be much less than 100 fA based on equation (4.1). For a higher G , the requirement for I_b is more stringent—too much so for a real integrated chip. A resistor with a lower resistance should be paralleled with the ME sensor to reduce this critical requirement of I_b . However, too large a resistance in this parallel configuration will degrade the performance of the ME sensor, since it will introduce Johnson noise which comes from the thermal agitation of electrons in a conductor. The rms Johnson noise voltage can be calculated by the following equation [16]:

$$V_t = \sqrt{4kTR\Delta f} \quad (4.2)$$

where k is Boltzmann's constant, T is the absolute temperature in kelvin, R is the resistance of the resistor in ohm and Δf is the noise bandwidth in hertz.

To achieve a flat ME response for the detection down to 1 mHz by the use of an instrumentation amplifier connected to the ME sensor in figure 1, a resistance greater than $4.2 \times 10^{10} \Omega$ is required to be put in parallel to the sensor, as given by equation (3.2) and figure 4. This high resistance would introduce Johnson noise with a spectral voltage noise density of $26 \mu\text{V Hz}^{-1/2}$, which is too large and will deteriorate the performance of the ME detection system (since most instrumentation amplifiers will induce only tens of $\text{nV Hz}^{-1/2}$ noise referred to the input). For ME sensors with lower capacitance, a flat ME response at low frequency will require even higher input resistances (a ME sensor with 10 pF capacitance will require a parallel resistance of $>16 \text{ T}\Omega$ for $f_c = 1 \text{ mHz}$). In this case, the I_b requirement given by (4.1) will be more stringent and for the requirement of a flat ME response below 1 mHz, a larger parallel resistor will also be needed; however, these will degrade the performance of the ME detection system.

A third method for the ME sensor detection is the use of a charge amplifier. The equivalent scheme for a charge amplifier connected to a ME laminate sensor is given in figure 6(a), where C_a and R_a are simply the input capacitance and resistance of the operational amplifier (op-amp) and C_f is the feedback capacitance. Because of the Miller effect, the equivalent scheme can be redrawn, as given in figure 6(b), where $C_m = (1 + g)C_f$ and g is the open loop gain of the op-amp. Ideally, $g = \infty$ but practically, it is finite (but large) at low frequency. Because g is very large ($\sim 10^5$ at low frequency), we have $C' \approx C_m$. The transfer function is then

$$H_2(s) = \frac{s \cdot g \cdot \alpha \cdot R'}{1 + s \cdot R' \cdot (1 + g) \cdot C_f}, \quad (5.1)$$

where $R' = R_0/R_a$. The corner frequency is $f_1 = 1/[2\pi R'(1 + g)C_f]$. By assuming $g = 10^5 \text{ V/V}$, $C_f = 100 \text{ pF}$ and $R' > 1 \text{ T}\Omega$ (by choosing an op-amp with a high input impedance larger than 1 T Ω), we can estimate the high corner frequency to be as low as 1.6 μHz . However, there is also an I_b consideration in charge amplifier design—as in figure 6(a), the bias current I_b will saturate the op-amp's output. This

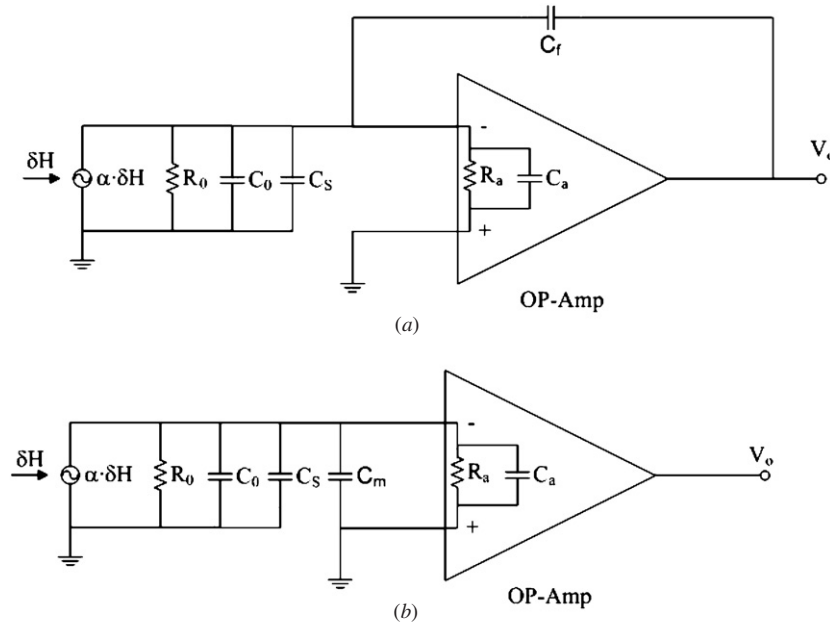


Figure 6. Equivalent scheme for ME laminate with a charge amplifier: (a) conventional representation and (b) simplification of scheme using Miller effect.

saturation can be solved by (i) paralleling a large feedback resistor R_f with the feedback capacitor C_f [17] or (ii) using an auto-bias dc servo circuit [18]. Here, for simplification, we have chosen the first.

To acquire a flat ME response down to 1 mHz, R_f should be chosen to satisfy the following

$$\frac{1}{2\pi R_f C_f} < 1 \text{ mHz.} \tag{5.2}$$

For $C_f = 100$ pF, R_f should be chosen to be larger than 1.6 TΩ; for $C_f = 1$ nF, R_f should be chosen to be larger than 160 GΩ. Furthermore, the requirement for the op-amp’s bias current I_b to avoid saturation should satisfy the following

$$I_b \ll \frac{V_s}{R_f}, \tag{5.3}$$

where V_s is the saturation output voltage of the op-amp (we choose $V_s = 3$ V for convenience). For $R = 1.6$ TΩ, I_b should be less than 2 pA; for $R = 160$ GΩ, I_b should be less than 20 pA. From the above analysis, we can see that the I_b requirement of the charge amplifier is much lower than that of the instrumentation amplifier. Furthermore, $R = 1.6$ TΩ introduces thermal noise with a spectral current noise density of about 0.1 fA Hz^{-1/2} which is much lower than the spectral current noise density of most operational amplifiers. Accordingly, the introduction of this high value feedback resistance will not degrade the performance of the ME detection system. Furthermore, we can also see that the I_b requirement will not change even if we use the charge amplifier detection method with ME sensors having much lower capacitances (such as 10 pF). In a prior report, we used a charge method to detect the ME signal down to frequencies in the milli-Hz range [19].

From the above analysis, we can see that a charge scheme for a ME laminate sensor is superior for the detection of

magnetic field variations at low frequencies. Using said detection circuitry, the frequency response characteristics of ME laminates are flat for frequencies down to 1 mHz, that is without introducing significant noise and increasing the requirement of the ME sensor capacitance. Such low noise flat ME response characteristics are essential for magnetic anomaly detection in the quasi-static frequency range.

4. Noise considerations in the ME laminate detection by a charge amplifier

Let us then consider the modification of the low frequency equivalent circuit of figure 6(a) by inclusion of an ultra-low bias-current op-amp. Figure 7(a) shows such an equivalent scheme, where $R_1 = R_0 R_a / (R_0 + R_a)$ is the lumped parallel resistance, $C_1 = C_0 + C_s + C_a$ is the lumped parallel capacitance, and R_1 and C_1 are the feedback resistance and capacitance of the op-amp, respectively. The transfer function $H_3(s)$ of the output voltage $V_o(s)$ to the input ac magnetic fields $H(s)$ of the equivalent scheme in figure 7(a) can be given as

$$H_3(s) = \frac{V_o(s)}{H(s)} \cong \frac{\alpha \cdot s \cdot R_1}{1 + s \cdot R_1 \cdot C_1}. \tag{6}$$

For $f > f_1$, the high frequency gain is $|H(s)| = \frac{\alpha}{C_1}$. To achieve a high gain, C_1 should be small, but yet too small a C_1 will increase the low corner frequency f_1 . In order to avoid stray capacitance and equivalent noise, C_f should be at least ≥ 10 pF [20].

We next performed an equivalent noise analysis of the scheme in figure 7(a), as illustrated in the model of figure 7(b), where i_{ni} and i_{n1} are the spectral current noise densities of the ME sensor and R_1 respectively; and i_n and e_n are the spectral current and voltage noise densities of the op-amp, respectively. The spectral current noise densities of the various resistors can

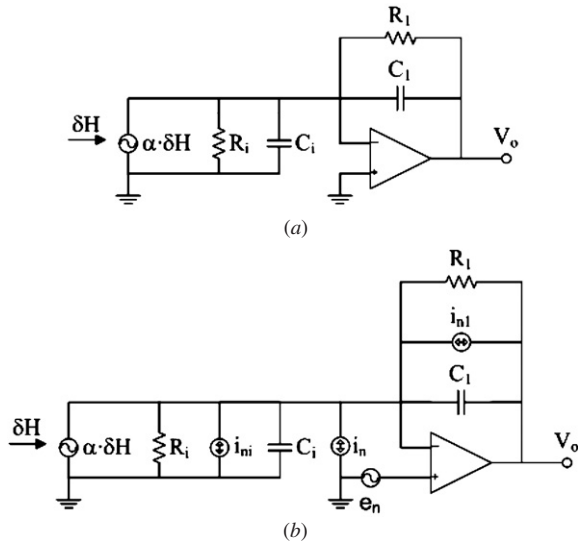


Figure 7. (a) Equivalent scheme for low frequency ME laminate detection using op-amp and (b) the noise model of this equivalent scheme.

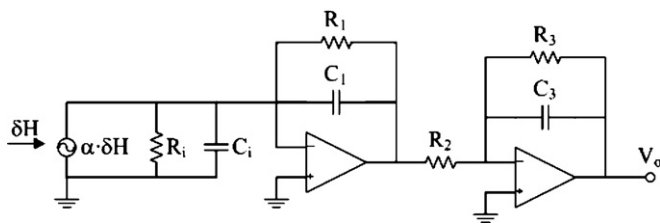


Figure 8. Equivalent scheme, including a low-pass filter.

be assumed here to be constituted of only thermal noise, given as $i_n = (4 kTR^{-1})^{0.5}$ [16]. The values of i_n and e_n can be acquired from the op-amp datasheet; we recommend FET-type input op-amps, both for their low bias current I_b and low

current spectral noise density i_n in this high impedance source sensor measurement.

There are two noise gains to be concerned within the scheme of figure 7(b): one is the current noise gain $Z_{n1}(s)$ for the spectral current noise density of i_{ni} , i_{n1} and i_n and another is the voltage noise gain $A_{n1}(s)$ for the spectral voltage noise density e_n . The gains $Z_{n1}(s)$ and $A_{n1}(s)$ can readily be shown to be

$$Z_{n1}(s) \cong \frac{R_1}{1 + s \cdot R_1 \cdot C_1} \quad (7.1)$$

$$A_{n1}(s) \cong \frac{1}{\beta(s)} = \left(1 + \frac{R_1}{R_i}\right) \cdot \frac{1 + sR'C'}{1 + s \cdot R_1 \cdot C_1}, \quad (7.2)$$

where β is a feedback factor of the circuit and $R' = R_1R_i/(R_1 + R_i)$ and $C' = C_1 + C_i$. To restrict noise amplification and stabilize low-frequency detection capabilities, we next introduced a low-pass filter on the output side, as illustrated in figure 8. The transfer function $H_s(s)$ of the signal in the scheme of this figure, including the current noise gain and voltage noise gain given in (7.1) and (7.2), now becomes

$$H_s(s) = \frac{V_o(s)}{H(s)} \cong -\alpha \cdot \frac{R_3}{R_2} \cdot \frac{s \cdot R_1}{(1 + s \cdot R_1 \cdot C_1) \cdot (1 + s \cdot R_3 \cdot C_3)} \quad (8.1)$$

$$Z_n(s) = -\frac{R_3}{R_2} \cdot \frac{R_1}{(1 + s \cdot R_1 \cdot C_1) \cdot (1 + s \cdot R_3 \cdot C_3)} \quad (8.2)$$

$$A_n(s) = -\frac{R_3}{R_2} \cdot \left(1 + \frac{R_1}{R_i}\right) \cdot \frac{1 + sR'C'}{(1 + s \cdot R_1 \cdot C_1) \cdot (1 + s \cdot R_3 \cdot C_3)}. \quad (8.3)$$

The Bode plot for $|H_s(j\omega)|$ is given in figure 9(a). Inspection of this figure will reveal that the bandwidth of ME

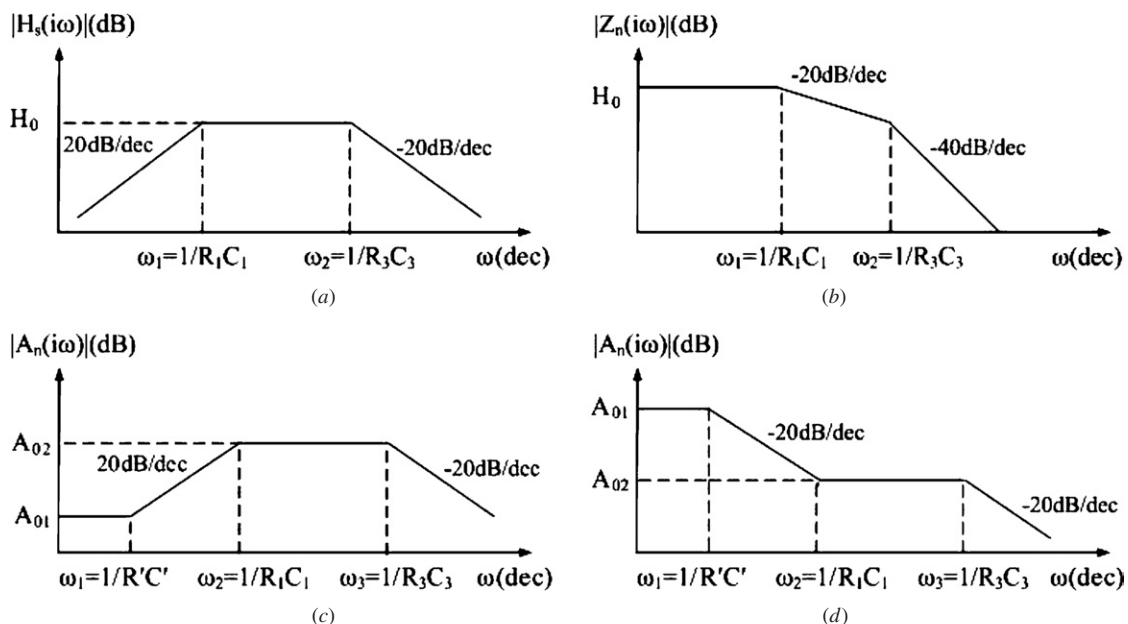


Figure 9. Bode plots of (a) $|H_s(s)|$, (b) $|Z_n(s)|$, (c) $|A_n(j\omega)|$ for $R_iC_i > R_1C_1$ and (d) $|A_n(j\omega)|$ for $R_iC_i < R_1C_1$.

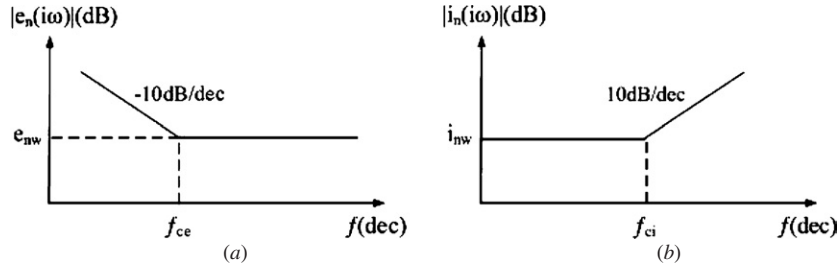


Figure 10. Typical spectral noise density of a FET: (a) voltage and (b) current.

detection is restricted to $1/(2\pi R_1 C_1) < f < 1/(2\pi R_3 C_3)$, i.e., there are both low and high corner frequencies. Bode plots of the noise gain $|Z_n(j\omega)|$ are given in figure 9(b) and those of $|A_n(j\omega)|$ in figures 9(c) and (d) for the conditions $R_i C_i > R_1 C_1$ and $R_i C_i < R_1 C_1$, respectively. Generally, $R_i C_i$ is larger than $R_1 C_1$ for ME laminate detection, meaning that we only need to consider the case of figure 9(c) where

$$H_0 = \frac{R_3}{R_2} \cdot \frac{\alpha}{C_1}, \quad Z_0 = \frac{R_3}{R_2} \cdot R_1,$$

$$A_{01} = \frac{R_3}{R_2} \cdot \left(1 + \frac{R_1}{R_i}\right) \quad \text{and} \quad A_{02} = \frac{R_3}{R_2} \cdot \left(1 + \frac{C_i}{C_1}\right).$$

To achieve the lowest signal detectivity, we can fix the signal gain H_0 , and then consider the noise gain Z_n or A_n . The only component we can adjust is R_1 as we fixed H_0 ; however, from figures 9(b) and (c), we can see that the choice of a suitable R_1 is not easy. To solve this problem, we need to consider the total expression for the noise and find its minimum. As we have mentioned above, a FET type op-amp is the best choice in such designs. Spectral noise densities for $e_n(f)$ and $i_n(f)$ are illustrated in figure 10 and can be given as [16]

$$e_n = e_{nw} \left(1 + \frac{f_{cc}}{f}\right)^{1/2}; \quad i_n = i_{nw} \left(1 + \frac{f}{f_{ci}}\right)^{1/2}, \quad (9)$$

where e_{nw} and i_{nw} are the white noise floors and f_{cc} and f_{ci} are the corner frequencies.

For a spectral voltage noise density $e_{ni}(f)$ with a noise gain of $A_n(jf)$ and a spectral current noise density $i_{ni}(f)$ with a noise gain of $Z_n(jf)$, the output RMS noise contributions from these two sources can be independently calculated to be [16, 17]

$$E_{noe} = \left(\int_{f_L}^{f_H} |A_n(jf)|^2 e_{ni}^2(f) df \right)^{1/2} \quad (10.1)$$

$$E_{noi} = \left(\int_{f_L}^{f_H} |Z_n(jf)|^2 i_{ni}^2(f) df \right)^{1/2}. \quad (10.2)$$

The total RMS noise can then be calculated from the root-square summation of the noise sources [16]; we assume here that the noise sources are uncorrelated. The total output RMS noise is

$$E_{noT} = \sqrt{E_{noe}^2 + E_{noi}^2}$$

$$= \left(\int_{f_L}^{f_H} |Z_n(jf)|^2 i_{ni}^2(f) df + \int_{f_L}^{f_H} |A_n(jf)|^2 e_{ni}^2(f) df \right)^{1/2}$$

$$= \frac{R_3}{R_2} \times \left\{ \int_{f_L}^{f_H} \left| \frac{R_1}{\left(1 + \frac{jf}{f_1}\right) \cdot \left(1 + \frac{jf}{f_3}\right)} \right|^2 \left[\frac{4kT}{R_1} + \frac{4kT}{R_i} \right. \right.$$

$$\left. \left. + i_{nw}^2 \left(\frac{f}{f_{ci}} + 1 \right) \right] df + \left(1 + \frac{R_1}{R_i} \right)^2 \cdot e_{nw}^2 \right.$$

$$\left. \cdot \int_{f_L}^{f_H} \left| \frac{1 + \frac{jf}{f'}}{\left(1 + \frac{jf}{f_1}\right) \cdot \left(1 + \frac{jf}{f_3}\right)} \right|^2 \left(\frac{f_{cc}}{f} + 1 \right) df \right\}^{1/2} \quad (11)$$

where $f_1 = (2\pi R_1 C_1)^{-1}$, $f_3 = (2\pi R_3 C_3)^{-1}$, $f' = (2\pi R' C')^{-1}$, $R' = R_1 R_i / (R_1 + R_i)$ and $C' = C_1 + C_i$. For a finite measurement time T_m , we can approximate $f_L = 1/T_m$. From (11), we can see that E_{noT} is decreased when $i_{nw}(e_{nw,cc})$ decreases or when R_i (f_{ci}) increases. Thus, we can see that the noise of a magnetic field detection system can be lowered by choosing an op-amp with low $i_{nw}(e_{nw,cc})$ and high f_{ci} , or by designing a ME laminate with higher dc resistance.

5. Prototype unit

We then constructed a prototype ME detection system consisting of the low noise detection circuit that we designed in figure 8 and a ME laminate sensor configuration that we constructed in figure 1. The PCB prototype is constructed by using the etching method and can be referred to [21]. The detection scheme was based on the charge amplifier method of sections 3 and 4. A photograph of this passive magnetic field detection system is given in figure 11.

We chose a polypropylene capacitor for C_1 , due to its very low leakage current and lack of memory effect at low frequencies. The following values are typical of the electrical parameters used in the detection circuit: $C_1 = 100$ pF, $R_2 = 1$ k Ω , $R_3 = 100$ k Ω , $C_3 = 100$ nF. We chose LMC660 as the main chip due to its high performance and inexpensive nature. A ME sensor is held in a Teflon tube here to prevent the leakage current. The output of figure 8 was followed by a circuitry with a gain of 10 that was used to amplify the output signal which was then fed into an oscilloscope (obscuring the oscilloscope's input noise); a fourth-order Butterworth low pass filter with a corner frequency of $f_c = 11$ Hz was

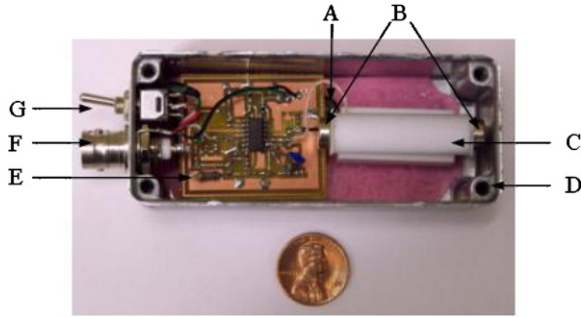


Figure 11. Photograph of the prototype ME detection system. A: batteries (below the PCB board); B: optimized dc magnetic bias (NbFeB); C: Teflon tube (ME sensor is held inside); D: aluminum box; E: low noise charge amplifier; F: output jack; G: power switch.

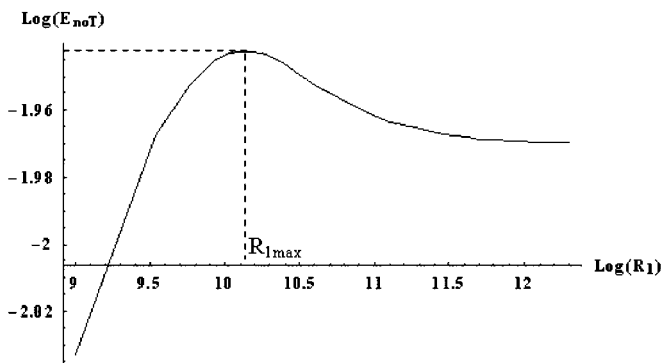


Figure 12. RMS noise E_{noT} as a function of input resistance R_1 .

also introduced at the output of figure 8, further reducing the 60 Hz noise. The measurement time was set as $T_m = 10$ s. We can then plot the total RMS noise E_{noT} of equation (11) as a function of the input resistance R_1 over the range of $10^9 \Omega < R_1 < 2 \times 10^{12} \Omega$, as illustrated below in figure 12. From this figure, we can see that E_{noT} initially increases with increasing R_1 , subsequently reaching a maximum at a value of $R_{1max} \approx 1.3 \times 10^{10} \Omega$ and then decreasing with further increment in R_1 .

A flat ME response requires that R_1 should satisfy the condition that $R_1 < 1/(2\pi f C_1)$, where f is the high corner frequency: for $f = 1$ mHz, this requires $R_1 > 1.6$ T Ω . Combining this with figure 12, we can determine that the larger the value of R_1 , the lower E_{noT} becomes. However, the limitation of I_b (discussed in section 3) requires that R_1 should not be greater than 1 T Ω . This design consideration is good in a laboratory environment, where vibration damping and shielding systems are available [19]; however, for practical (real world) usage, the choice of too large of an input resistance $R_1 (\geq T\Omega)$ will allow for the introduction of more low frequency environmental noise (i.e., vibration, pyroelectric effect, etc). As an alternative to help with the rejection of environmental noise sources, we could lower the choice of input resistance to $R_1 = 1$ G Ω . However, this in turn would deteriorate the low frequency performance of the ME detection system, although the methodology would still be viable for >1 Hz. In this regard, the design considerations are a compromising situation.

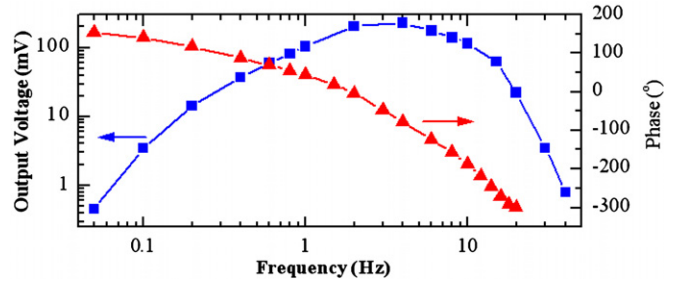


Figure 13. ME response of the ME unit.

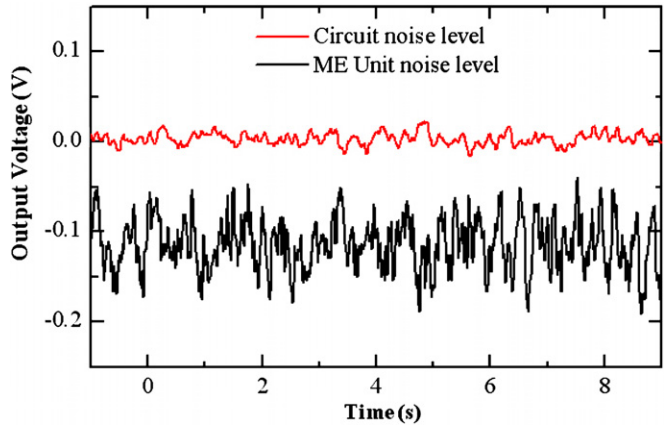


Figure 14. Output noise level of the detection circuitry and ME unit (circuit + sensor).

The detection circuitry we chose for the prototype of figure 11 was based on these compromised design considerations for R_1 . The ME output voltage and phase (with respect to the drive frequency) for this more practical alternative design ($R_1 = 1$ G Ω) are shown in figure 13, where a high pass filter (following section 3, figure 8) with a corner frequency of $f_{c1} = 0.16$ Hz was applied after the output, reducing further the low frequency environmental noise. During the measurement of the complex ME response [5, 6, 9, 19], an electromagnet was used to apply H_{dc} ; a pair of Helmholtz coils was used to generate a small H_{ac} ; and the induced voltage was measured by a lock-in amplifier. As can be seen from figure 13, the ME response decreased notably outside the frequency range of 1–10 Hz, and also the phase shift became more pronounced with increasing frequency.

We next measured the output voltage noise level from the detection circuit (disconnected the ME sensor) and the ME detection unit (circuit and sensor), which are given in figure 14, respectively. The RMS values of the equivalent output voltage noises were 8 mV and 30 mV respectively, using a crest factor of 5 to relate peak-to-peak and RMS values. From figure 12, we can then estimate that the equivalent RMS output voltage noise of the ME detection system excluding environmental noise should have been about 9 mV, which is notably less than the measured value. This discrepancy between the measured noise floor and our prediction shows that other intrinsic (radiation, dielectric loss, etc) and environmental (vibration, pyroelectric, etc) noise sources act on our ME sensor unit: introducing $\sim 3\times$ more noise than that of the detection circuitry, which we did not consider in equation (11).

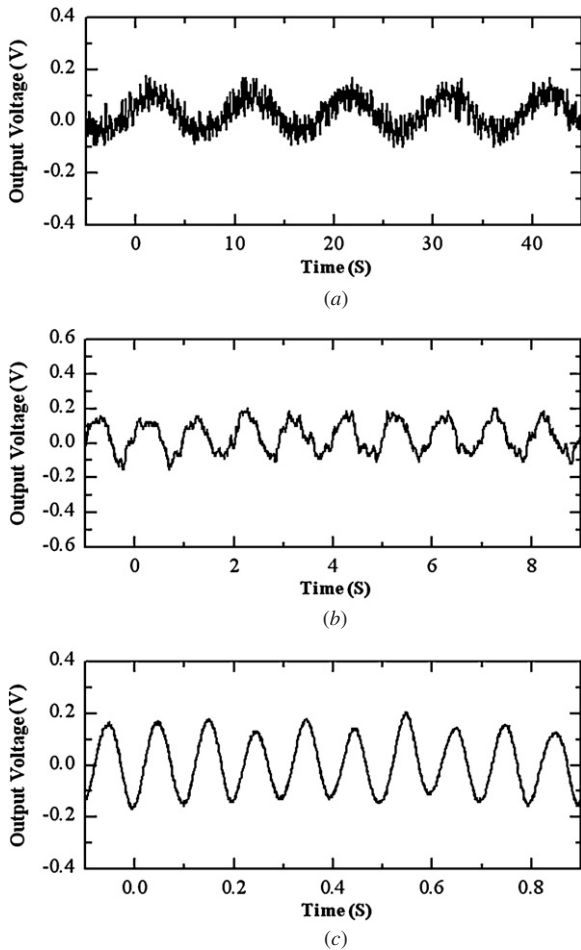


Figure 15. Response of system to different sinusoidal magnetic input signals: (a) 0.1 Hz, 26 nT input; (b) 1 Hz, 2.6 nT input; (c) 10 Hz, 2.6 nT input.

Further research needs to focus on considerations of the rejection of environmental noise, and subsequently on improved detection circuitry optimization.

Finally, we determined the sensitivity limits of our ME sensor unit to small variations in magnetic fields. To do this, we measured the voltage induced on the ME unit in response to an applied ac magnetic field in a time domain capture mode. These measurements were made outside a magnetically shielded environment, simply by taking the output voltage from the sensor unit (see figure 11) and inputting it into an oscilloscope (consistent with the noise analysis given above in sections 3 and 4). Measurements were made at various measurement frequencies. The response of our ME detection system (see photo in figure 11) to small magnetic field variations of 2.6 nT at 1 Hz and 10 Hz and of 26 nT at 0.1 Hz are then given in figure 15. These data represent a conservative estimate of the sensitivity limit of our ME sensor unit to small magnetic field variation that could be detected with a high degree of confidence at the respective frequencies in a time domain capture mode, without signal averaging or referencing to a known phase. We also did the simple tests (data not shown) of measuring the peak-to-peak voltage noise of the detection circuitry (without ME laminate) under large

magnetic field environment (1 mT) in a time domain capture mode: as expected, the results were similar to those shown in figure 14 (top); this gave us confidence of good magnetic inertness of the circuit. Comparisons of the data in figure 15 to the peak-to-peak voltage noise of figure 14 (bottom) (for the ME sensor unit) clearly demonstrate the ability of our ME sensor unit to detect minute magnetic field variations using the charge amplifier scheme presented in sections 3 and 4.

6. Summary

Here, we have presented a ME detection technology including ME laminate equivalent circuit model, detection circuitry and noise mitigation for sensing small magnetic field variations of quasi-static frequencies. With regards to the detection circuitry, we have shown that a charge detection methodology is more effective than a voltage one. Using said detection circuitry, the frequency response characteristics of the ME unit are flat for $f > 1$ mHz. With regards to noise mitigation, we have developed an effective equivalent scheme which limits the bandwidth to a suitable range for the detection of small magnetic anomalies of low frequencies in a time-domain capture mode. We then constructed a prototype unit, and our ME prototype unit can detect a magnetic signal as small as 2.6 nT at a frequency of 1 Hz. This technology is small and passive.

Acknowledgment

We are grateful to the Office of Naval Research for supporting this research effort.

References

- [1] Landau L D and Lifshitz E M 1960 *Electrodynamics of Continuous Media* (Oxford: Pergamon) p 119
- [2] Fiebig M 2005 *J. Phys. D: Appl. Phys.* **38** R123
- [3] Ryu J, Carazo C Z, Uchino K and Kim H E 2001 *Japan. J. Appl. Phys.* **40** 4948
- [4] Bichurin M I, Filippov D A and Petrov V M 2003 *Phys. Rev. B* **68** 132408
- [5] Dong S X, Li J F and Viehland D 2003 *Appl. Phys. Lett.* **83** 2265
- [6] Dong S X, Li J F and Viehland D 2003 *IEEE Trans. Ultrason. Ferroelectr. Freq. Control* **50** 1253
- [7] Nan C W, Cai N, Shi Z, Zhai J, Liu G and Lin Y 2005 *Phys. Rev. B* **71** 014102
- [8] Srinivasan G, Hayes R and Devreugd C P 2005 *Appl. Phys. A—Mater. Sci. Process* **80** 891
- [9] Xing Z P, Dong S X, Zhai J Y, Li J F and Viehland D 2006 *Appl. Phys. Lett.* **89** 112911
- [10] Nan C W 1994 *Phys. Rev. B* **50** 6082
- [11] Lenz J E 1990 *Proc. IEEE* **78** 973
- [12] Caruso M J and Withanawasam L S Vehicle Detection and Compass Applications using AMR Magnetic Sensors. Honeywell, SSEC, 12001 State Highway 55, Plymouth, MN, USA 55441, <http://www.ssec.honeywell.com>.
- [13] Cullity B D 1972 *Introduction to Magnetic Materials* (Cambridge, MA: Addison-Wesley)
- [14] Baxter L K 1997 *Capacitive Sensors* (New York: IEEE)
- [15] Petrov V M, Bichurin M I and Srinivasan G 2004 *Tech. Phys. Lett.* **30** 81

- [16] Motchenbacher C D and Connelly J A 1993 *Low Noise Electronic System Design* (New York: Wiley)
- [17] Franco S 2002 *Design with Operational Amplifiers and Analog Integrated Circuits* (New York: McGraw-Hill) p 21
- [18] Analog Devices, Inc., AD745 Data sheets, www.analog.com, 2002
- [19] Dong S X, Zhai J Y, Xing Z P, Li J F and Viehland D 2005 *Appl. Phys. Lett.* **86** 102901
- [20] Keithley Instruments, Inc. 2004 *Low Level Measurement Handbook—Precision DC Current, Voltage, and Resistance Measurements*
- [21] Xing Z P 2004 *Expert Guidance: Protel99se* (Beijing: China Railway) pp 105–7